Mechanical properties and brittleness of shale with different degrees of fracturing-fluid saturation

Zhenkun Hou[1–3], Marte Gutierrez[2], Anming Wang[1,*], Abdulhadi Almrabat[2] and Chunhe Yang[3]

[1]College of Geosciences and Engineering, North China University of Water Resources and Electric Power, Zhengzhou 450045, China
[2]Department of Civil and Environment Engineering, Colorado School of Mines, Golden 80401, USA
[3]State Key Laboratory for Coal Mine Disaster Dynamics and Control, Chongqing University, Chongqing 400044, China

The mechanical characteristics of Longmaxi Formation shale with different degrees of fracturing-fluid saturation were characterized by applying triaxial compression tests at a confining pressure of 50 MPa. The test samples were collected from fresh outcrop shale in Dayou, Chongqing, China and the shale brittleness was evaluated based on brittleness-drop coefficient, stress decrease coefficient and softening modulus. The weakening of related rock parameters of shale specimens being immersed in fracturing-fluid for different time periods was studied and discussed. The degree of deterioration of the peak strengths, elastic and softening moduli and brittleness were significant and varied exponentially when the samples were soaked in fracturing-fluid. The samples were found to fail by shear on the whole accompanied by varying degrees of bedding plane cracking. With increase of sample immersion time, the number of shear failure surfaces changes from one to two and finally to more than three. The length and number of cracks parallel to bedding planes increased gradually, however, no cracks were formed perpendicular to the bedding plane even when the shale was soaked for a long time. The weakening of the brittleness and mechanical parameters with sample fracturing-fluid saturation are mainly related to change of stress state at the crack tips caused by hydration swelling, the dissolution caused by alkaline fracturing-fluid and the formation of liquid film on the surface of shale particles, all of which are the results of mechanical–physical–chemical coupling.

Keywords: Brittleness evaluation index, hydration swelling, immersion time, Longmaxi Formation shale, triaxial compression, weakening mechanism.

IN 2013, the United States Energy Information Administration (EIA) evaluated 137 shale formations in 41 countries other than United States (including China, Russia, Canada and other countries), and estimated the total resource of technically recoverable shale gas to be 2.07×10^{14} m^3, which accounts for 47% of the world's total natural gas resources[1]. The resource of technically recoverable shale gas in China is 3.608×10^{13} m^3 ranking it first in the world[2]. Due to the ultra-low permeability of shale, more than 90% of shale gas wells need to communicate with natural fractures through hydraulic fracturing to form highly permeable channels for commercial exploitation after completion of drilling[3–5]. During drilling, the drilling filtrate enters the shale formation along the bedding planes or micro-cracks pushed by capillary action and drilling pressure differentials. Physical and chemical reactions between drilling fluid and clay mineral particles take place, which produce hydration stress and reduce shale strength[6]. Many complicated drilling accidents such as sloughing, collapsing, pipe sticking, pipe packing and caving are caused by shale and aqueous filtration interactions[7,8], which eventually lead to breakout, collapse and other borehole wall stability problems[9,10]. According to relevant statistics, the global annual loss caused by wellbore instabilities is up to 10 billion dollars[11]. Wellbore stability is a technology bottleneck, which restricts the development of shale gas and other unconventional oil and gas resources[12].

Shale hydration and wettability have been studied in detail with interesting results. Studies about wellbore stability based on hydration characteristics can be divided into the following evolutionary stages: pure mechanics research[13], chemical research of drilling fluid[14], coupled mechano-chemical research[15] and thermo-hydro-mechanical–chemical–electrical multi-field coupled research[16]. In recent years, some new materials like inhibitors and blocking agents such as polyethyleneimine[17] and zizyphus spina-christi extract[18] are being applied into drilling construction sites. With the advancement in science and technology, new methods, such as CT computerized tomography[7], nuclear magnetic resonance[19] and microscopic examinations (such as mercury intrusion porosity testing, nitrogen adsorption tests)[20,21], are also used to study hydration characteristics of shale and changes of mineral composition and microstructure of shale after hydration.

*For correspondence. (e-mail: wam992001@163.com)

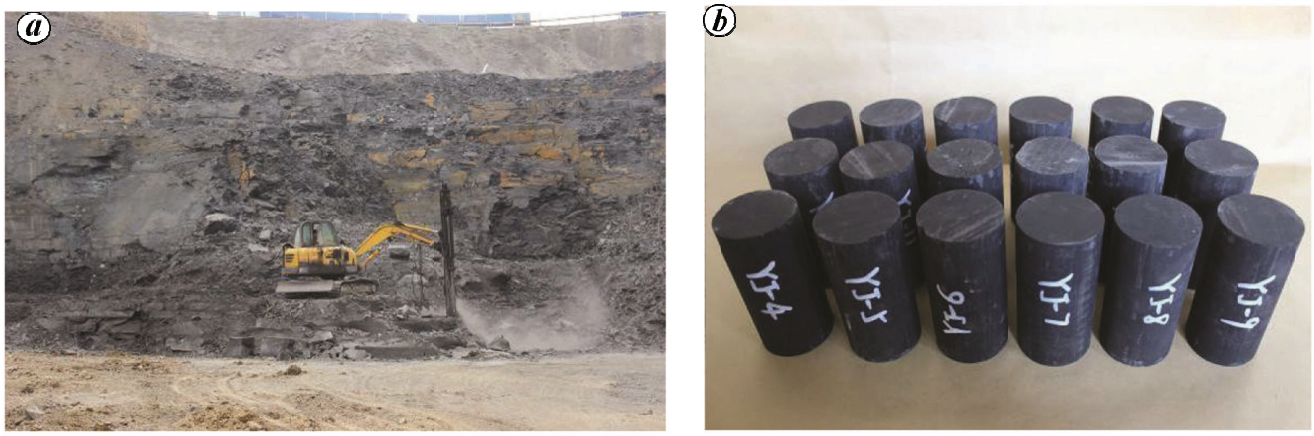

Figure 1. Test materials: ***a***, Test material sampling site. ***b***, Part of test samples.

Shale hydration not only affects wellbore stability, but also the fracturing construction process. The capillary effect and closure of natural fractures lead to a low flow-back rate of fracturing-fluid. The average flow-back rate is about 20–40% in US and less than 5–10% in some of the shale gas wells of shale gas blocks of Fuling in Chongqing, China[22,23]. Long-term retention of fracturing-fluid in shale reservoirs can change the physical and mechanical characteristics and the brittleness of shale, affecting the fracturing effect later. However, there are few studies on mechanical parameters and brittleness characteristics of shale under high confining pressure and under different immersion times of fracturing-fluid[24].

The brittleness of shale can significantly affect wellbore stability, fracturing response, cap rock integrity, etc.[25,26]. Although about 20 different quantitative methods for evaluation of brittleness have been proposed based on mineral constituents, hardness, full stress–strain curve, energy, logging curve, fracture toughness, pump pressure curve, expansion inflection point, etc., there is no unified understanding regarding the shale brittleness evaluation method[27–32]. Most of the above methods are presented based on the objective of the study, with the result there is a lack of uniform and comprehensive approach to characterize the brittleness of shale. It is usually perceived that brittleness depends only on the rock and is an inherent property of the rock. In fact, brittleness is a complex rock characteristic and cannot be represented simply by a single variable or rock's physical and mechanical property. It is also closely related to external conditions such as confining pressure, temperature, pore fluid properties and intrusion and loading rate[26,33].

In order to study the mechanical properties and brittleness characteristics of shale under different durations of immersion in a fracturing-fluid, triaxial compression on specimens of Longmaxi Formation from Dayou in China were tested under a confining pressure of 50 MPa. A quantitative evaluation of a comprehensive brittleness index, which could broadly reflect the loss of load-bearing capacity and the ability to resist inelastic deformation, was established based on brittleness-drop coefficient, stress decrease coefficient and softening modulus. The effects of different sample immersion durations in a fracturing-fluid, and high confining pressure–temperature coupling on the mechanical parameters and brittleness of shale were studied. The results provide some important insights into hydraulic fracturing, wellbore stability, evaluation of shale gas reservoirs, selection of perforated section and fracturing design in shales, and cap rock integrity.

Test materials and procedures

Test material

The test samples were collected from fresh outcrop shale in Chongqing, China. Outcrop is a natural extension of a shale gas reservoir in the shale gas blocks of Fuling in Chongqing. As shown in Figure 1 *a*, in order to ensure that samples were relatively fresh, core sampling was obtained from more than 30 m below the surface, and the collected large pieces of shale were immediately sealed with preservative cling film and wax paper.

In the laboratory, the test samples were drilled along the direction of shale bedding plane and prepared as standard rock mechanical test samples with a diameter of 50 mm and height of 100 mm (ref. 34; Figure 1 *b*). The allowable deviation of the diameter and the unevenness of both ends of the specimen are less than 0.2 mm and 0.05 mm respectively. The vertical deviation between the end face and axis is controlled at within ±0.25°. In order to reduce the individual differences, all test specimens were taken from the same location.

Preparation of the fracturing-fluid

The fracturing-fluid used in the tests is the same as the one employed in a shale gas reservoir well in Fuling district. It contained a drag reducer quality fraction of 0.1%, anti-swelling agent quality fraction of 0.2%, synergistic agent quality fraction of 0.1%, defoamer quality fraction of 0.02% and water. The fracturing-fluid has advantages of low damage, low viscosity, low friction, anti-swelling and dynamic floating.

Test methods and procedure

According to the data from Fuling district and Jianghan Oil Field, the *in situ* horizontal stress at the site was about 50 MPa and the formation temperature was about 80°C (ref. 35). In order to simulate the real formation conditions, shale samples were soaked in fresh fracturing-fluid at 80°C. To determine the effect of the degree of fracturing-fluid saturation, different samples were immersed at different times (t) 0, 2 and 8 h, and 1, 3 and 5 days. After soaking, triaxial compression tests were carried out on MTS815 loading machine using axial displacement control with a loading rate of 1×10^{-5} s^{-1} and the confining pressure was set to 50 MPa.

The steps followed in the experiments were: (1) preparing the fracturing-fluid according to actual quality fractioning practice; (2) sealing the fracturing-fluid to prevent evaporation; (3) heating the sealed fracturing-fluid in an oven at 80°C; (4) soaking the samples once fracturing-fluid temperature reached 80°C and (5) conducting triaxial compression test after soaking the sample for t hours.

Analysis of test results

Stress and strain response

Figure 2 shows the deviatoric stress–strain curves of soaked shale at different immersion times t. These curves have clear initial concave-up compression phases. The longer the sample saturation time, the more obvious the compaction phase, indicating that the micro-cracks within the shale gradually develop and expand, resulting in larger initial damage of shale with the increase of t. When $t = 0$ h, the curves have longer elastic stage, larger peak strength and residual strength, but the yield stage is not obvious. After reaching the peak strength, the curves drop rapidly. At this point, failure is a non-stable fracture propagation type, i.e. the test machine no longer produces work, and the released energy of the specimen itself makes fractures continue to expand uncontrollably. This process is unstable, indicating that shale has a high brittleness and is suitable for hydraulic fracturing. With the increase of t, the elastic phase gradually becomes shorter, and the plastic phase becomes longer. The elastic modulus, peak and residual strengths gradually decrease. After reaching the peak strength, the stress decrease rate slows down rapidly. The brittleness of the shale is weakened and its ductility is enhanced. This is because, a series of physical and chemical reactions take place between siliceous minerals and fracturing-fluid (discussed in the later sections). The grain structure of shale is damaged and the bonding between mineral particles is weakened, resulting in a decrease in cohesion and internal friction angle of shale. The micro-cracks within the shale gradually develop and expand under the action of capillary force and hydration stress. Thus, mechanical parameters and brittleness characteristics of the shale show the phenomenon of weakening.

Mechanical properties of shale soaked in fracturing-fluid

The mechanical properties of shale under different immersion times t are shown in Table 1 in terms of peak strength σ_a, residual strength σ_r, elastic modulus E, softening modulus M and Poisson's ratio μ.

Figure 3 *a* shows the mean of peak strength (σ_a) versus immersion time t curve. As can be seen, σ_a decreases with increase of t. When $t = 0$ h, σ_a is as high as 211.79 MPa. When $0 < t \le 72$ h, σ_a decreases almost linearly. When $t \ge 72$ h, the decrease rate of σ_a gradually slows down and σ_a finally stabilizes at (about) 113.49 MPa. Thus σ_a is reduced by 46.414%, which indicates that shale is damaged under hydration swelling. In Figure 3 *a*, σ_a varies exponentially with t with the following best-fit equation

$$\sigma_a = 99.13\exp(-t/14.13) + 114.02,\ R^2 = 0.937. \quad (1)$$

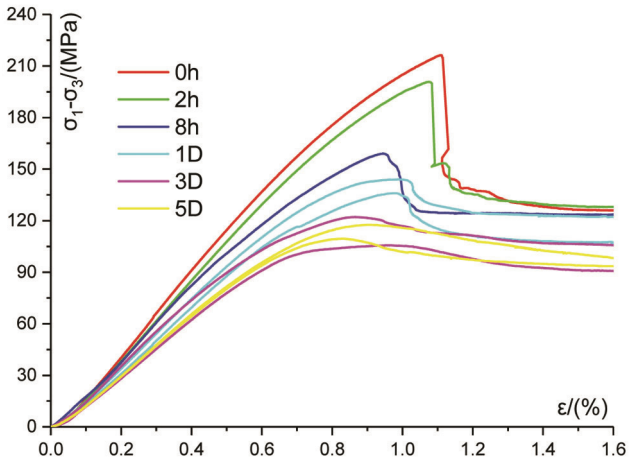

Figure 2. Deviatoric stress–strain curves of soaked shale (h, hours; D, days; confining pressure: 50 MPa).

Table 1. Mechanical parameters of shale under different fracturing-fluid immersion times

Test number	Peak strength σ_a/(MPa)	Residual strength σ_r/MPa	Elastic modulus E/(GPa)	Softening modulus M/GPa	Immersion time t
0 h–1	207.35	124.17	24.67	–70.76	0 h
0 h–3	216.23	138.33	23.09	–93.11	0 h
2 h–4	200.40	131.47	21.62	–31.75	2 h
2 h–6	212.52	114.67	22.98	–56.21	2 h
8 h–7	158.70	125.06	20.39	–24.85	8 h
8 h–9	162.15	113.41	23.47	–66.41	8 h
1 D–10	135.99	112.19	19.01	–12.67	1 D
1 D–11	143.88	124.13	18.98	–8.06	1 D
3 D–13	122.02	99.52	18.09	–1.79	3 D
3 D–14	105.57	90.56	16.64	–1.90	3 D
5 D–16	117.57	96.04	17.90	–2.55	5 D
5 D–17	109.40	95.27	16.98	–2.67	5 D

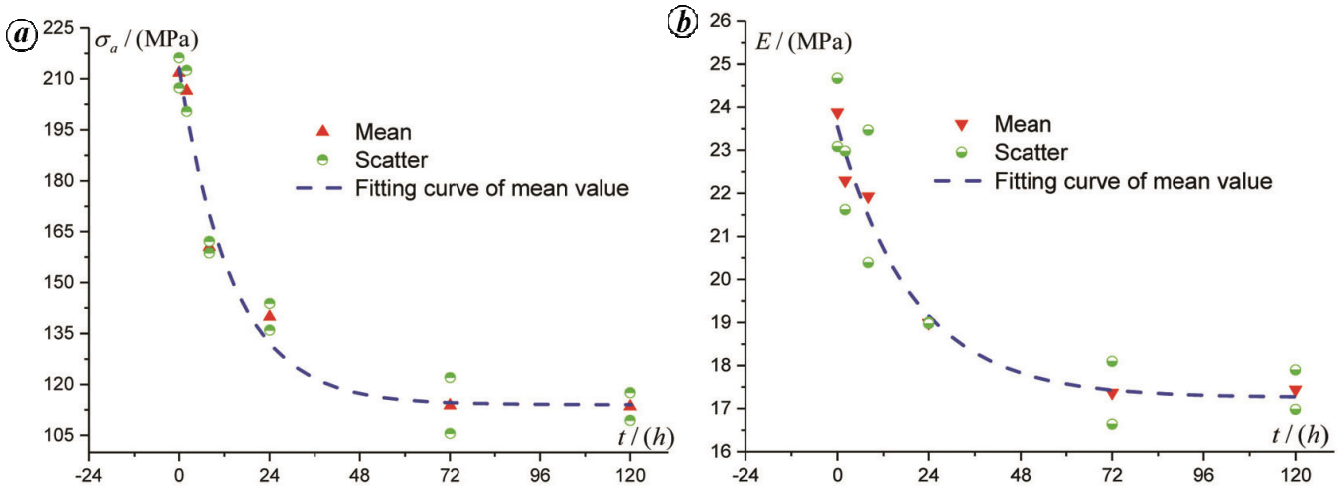

Figure 3. The changing laws of mechanical parameters of shale after being soaked (confining pressure = 50 MPa): ***a***, Mean of peak strength versus immersion time curve; ***b***, Mean of elastic modulus versus immersion time curve.

Figure 3 *b* shows the mean of elastic modulus (E) versus immersion time t, which is similar to the variation seen with σ_a. At the beginning of the curve, plot of E is dispersed. With increasing t, the data variability is significantly reduced as the effect of hydration swelling becomes more pronounced. When $t = 0$ h, E is as high as 23.88 GPa. When $0 > t \le 72$ h, E decreases almost linearly with time. When $t \ge 72$ h, the decreasing rate of E gradually slows down and E finally stabilizes at about 17.44 GPa, corresponding to a modulus degradation as high as 26.968%. Here, E varies exponentially with t with the best-fit equation

$$E = 6.29\exp(-t/20.04) + 17.26,\ R^2 = 0.974. \quad (2)$$

It can be seen from eqs (1) and (2) that both peak strength and elastic modulus vary exponentially with immersion time with a best-fit equation. We can use these best-fit equations to predict the peak strength and elastic modulus of shale during hydraulic fracturing for extracting shale gas and the brittleness of shale can then be calculated, which is useful for adjusting the hydraulic fracturing scheme.

As shown in Figure 4, both the mean of softening modulus $|M|$ and that of residual strength σ_r, exhibit a variation pattern similar to σ_a with increasing immersion time. Softening modulus M is the slope of the stress–strain curve from peak strength to residual strength, representing energy-release capacity after the damage of shale whereas elastic modulus is the slope of the stress–strain curve in the elastic phase, representing the ability of storing energy before the destruction of shale. Greater the value of E and $|M|$, more is the brittleness of shale. As can be seen from Figure 4, the value of $|M|$ is reduced from 81.94 GPa to 2.61 GPa, corresponding to a deterioration as high as 96.815%. Similarly, σ_r is reduced from 131.25 MPa to 95.66 MPa, with a degradation of 27.12%.

Effect of hydration swelling on the failure characteristics of shale

As shown in Figure 5, after different immersion times, the shale failure eventually becomes shear failure on the whole, accompanied by varying degrees of bedding plane cracking. Cracks parallel to bedding planes are produced by the soaking effect of fracturing-fluid, and whose length and number are increased with t. However, there was no crack formation perpendicular to the bedding planes even if the shale was soaked in fracturing-fluid for a long time. When $t = 0$ h, the failure mode of shale was a typical single plane shear failure and no bedding plane cracking was found. When $t = 2$ h, the failure mode was still a typical single plane shear failure, but bedding plane cracking was observed, albeit in a small number. When $t = 8$ h and $t = 1$ day, the number of shear surfaces increased from one to two, the length and number of cracks parallel to bedding planes increased, centering on the two end faces of the samples. When $t \geq 3$ days, the number of shear planes increased to more than three. The number of cracks also increased noticeably. All the cracks spread over the entire specimen and eventually formed a complex fracture network.

When t is smaller, the degree of cementation between bedding planes is stronger and the bedding plane is harder to be cracked. Eventually shale is more prone to shear failure under high confining pressure. However, with increase in t, the situation is opposite. Under hydration swelling, the degree of cementation between bedding planes, internal friction angle and cohesion decline gradually and the bedding plane is more likely to be cracked. Thus, in addition to increase in the number of shear planes, there are more cracks opening parallel to bedding planes.

To summarize, with increasing immersion time, the mechanical properties of shale experienced significant degradation. It took almost 72 h of soaking before degradation became complete. Hydration swelling can lead to significant decrease of peak strength, residual strength and elastic modulus, significant increase of the softening modulus and Poisson's ratio. Comparing the data from uniaxial and triaxial compression experiments[2,36], it was found that the effect of immersion time on mechanical properties of shale was more important than that of the bedding plane orientation and confining pressure. Therefore, studying the influence of hydration on the mechanical properties of shale is of practical significance to realize high efficiency and stable production of shale gas. In addition, influence of hydration on the failure modes of shale is also significant.

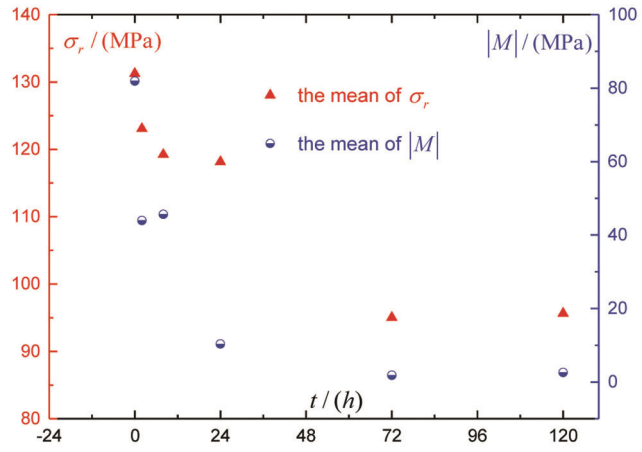

Figure 4. Mean of residual strength and that of the absolute value of softening modulus versus immersion time.

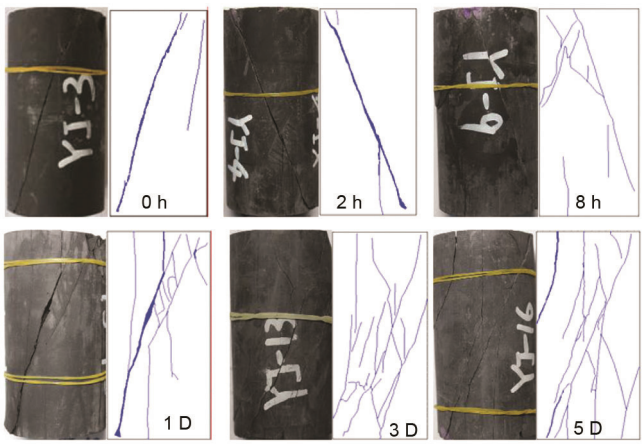

Figure 5. Failure modes of shale under triaxial compression test and after different immersion times in the fracturing-fluid.

Effect of hydration on the brittleness of shale

Brittleness is a comprehensive property of rock, which reflects an unsteady dynamic failure process under loading. A reasonable brittleness index should not only be able to express this characteristic but also the ability of a material to deform inelastically under unstable conditions. Shale brittleness can significantly affect wellbore stability and fracturing, which is important for selecting exact well section for perforation and designing fracturing scale.

Formulation of brittleness index parameters

The brittleness-drop coefficient R can be defined as follows (Figure 6)[37]

$$R = -(\varepsilon_B - \varepsilon_A)/(\varepsilon_M - \varepsilon_A), \tag{3}$$

where ε_A and ε_B are axial strains corresponding to peak strength σ_a and residual strength σ_r respectively. ε_M is the axial strain when the stress reaches σ_M at the time of loading and $\sigma_M = \sigma_r$.

From the generalized Hooke's law

$$\sigma_M = \sigma_r = E\varepsilon_M + 2\mu\sigma_3, \tag{4}$$

where E, μ and σ_3 are elastic modulus, Poisson's ratio and confining pressure respectively. The parameter ε_M can be obtained from eq. (4) as

$$\varepsilon_M = (\sigma_r + \sigma_3 - 2\mu\sigma_3)/E. \tag{5}$$

Figure 6 shows that lesser the value of R, more pronounced is the brittleness of rock. Hence, to a certain extent, R can reflect the brittleness of rock, which has been proved by relevant experiments[37,38]. However, it is not sufficient to express the brittleness of shale just by the brittleness-drop coefficient. The stress–strain curves of two types of brittle shale are shown in Figure 7 to illustrate this. Accordingly if we assume that $\varepsilon_{M1} = 4c$, $\varepsilon_{M2} = 6c$, $\varepsilon_{B2} = 9c$, $\varepsilon_{B1} = 10c$ and c is a constant, we can

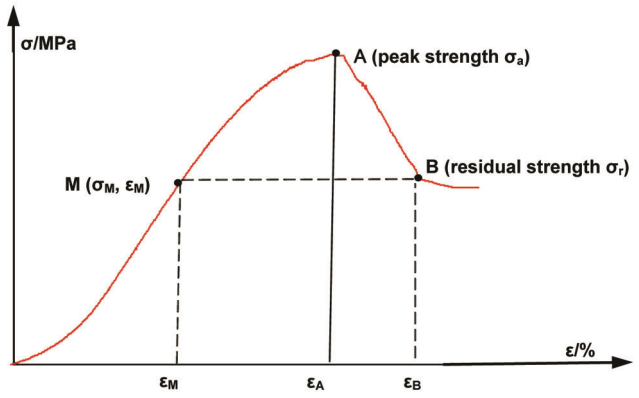

Figure 6. Complete stress–strain curve of a brittle rock (hypothetical curve).

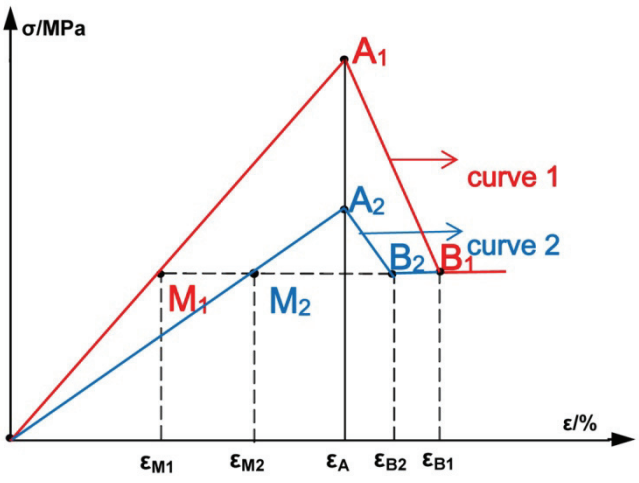

Figure 7. Stress–strain curves of two kinds of brittle shale (hypothetical curves).

then calculate the brittleness-drop coefficient of curves 1 and 2, which is 0.5 for both. However, the brittleness of curve 1 is stronger. Thus, the brittleness of shale is not only decided by R, but also depends on the stress decrease rate after the peak stress.

As shown in Figure 6, the slope of stress–strain curve from peak strength (A) to residual strength (B) is defined as the softening modulus M. To a certain extent, M can represent the stress decrease rate after the peak stress. M can be defined as

$$M = (\sigma_a - \sigma_r)/(\varepsilon_A - \varepsilon_B). \tag{6}$$

Depending on the value of M, shale brittleness can be divided into the following four categories (Figure 8; ref. 39): (1) ideal brittleness: $M \to -\infty$; (2) Ordinary brittle-plasticity: when $-\infty < M \le -E$, brittleness is stronger than plasticity; when $-E < M < 0$, plasticity is stronger than brittleness; (3) ideal plasticity: $M = 0$ and (4) strain-hardening: $M > 0$. When E is a constant, the brittleness of shale gradually increases with the decrease of M (Figure 8).

In Figure 8, although curves of category (2) (ordinary brittle plasticity), L_1 and L_2 have the same elastic modulus and stress decrease rate after peak stress, their brittleness is different since they have different stress decrease quantities after peak stress. Stress decrease is a phenomenon of stress reduction from peak strength to residual strength when the rock is damaged. It is generally believed that when the stress decrease rate is the same, greater the stress drop, stronger is the brittleness. From Figure 6, the stress decrease coefficient P can be defined as

$$P = (\sigma_a - \sigma_r)/\sigma_a. \tag{7}$$

Thus, brittleness is closely related to brittleness-drop coefficient, stress decrease coefficient and softening modulus. Brittle-drop coefficient can reflect the difficulty of brittle failure, while stress decrease coefficient and softening modulus can stand for the strength of brittleness.

Due to the strong brittleness of shale, it is difficult for strain-hardening phenomenon to appear. Therefore, only the first three cases ((1), (2) and (3)) in Figure 8, are analysed in this study. In order to establish a quantitative and comprehensive brittleness index, the brittleness indices corresponding to R, P and M, are defined as B_1, B_2 and B_3 respectively.

It can be seen from eq. (3) and Figures 6 and 8, that the range of R is $(0, +\infty)$. After normalization, the brittleness index B_1 corresponding to R can be defined as in eq. (8), where B_1 range is (0, 1).

$$B_1 = \exp(-R). \tag{8}$$

Substituting eqs (3) and (5) into (8), yields

$$B_1 = \exp\left[\frac{E(\varepsilon_B - \varepsilon_A)}{\sigma_r + \sigma_3 - 2\mu\sigma_3 - E\varepsilon_A}\right], \quad (9)$$

where ε_A, ε_B and ε_M are axial strains corresponding to points A, B and M respectively.

Since the range of the stress decrease coefficient P is (0, 1), its corresponding brittleness index B_2 can be directly defined as

$$B_2 = P. \quad (10)$$

Substituting eq. (7) into eq. (10), yields

$$B_2 = (\sigma_a - \sigma_r)/\sigma_a. \quad (11)$$

The range of B_2 is also (0, 1).

The range of softening modulus M of the first three cases in Figure 8 is $(-\infty, 0)$. After normalization, its corresponding brittleness index B_3 whose range is also (0, 1), can be defined as

$$B_3 = 1 - \exp(M/E). \quad (12)$$

Figure 8 shows that, from curve (1) (ideal brittleness) to (3) (ideal plasticity), the brittleness of shale gradually increases and plasticity decreases. At the same time, brittleness indices B_1, B_2 and B_3 increase gradually from 0 to 1, which shows that there is a positive correlation between them and the brittleness of shale. In other words, these indices can reflect the brittleness of shale. Greater the value of the three indices, stronger is the brittleness of shale. Based on these three parameters, the following comprehensive brittleness index B_d is proposed

$$B_d = \alpha B_1 + \beta B_2 + \gamma B_3, \quad (13)$$

where $\alpha + \beta + \gamma = 1$ and α, β and γ denote the relative weights of B_1, B_2 and B_3 in B_d respectively. The values of α, β and γ can not only be considered according to the same standard, but also according to different purposes or applications. Substituting eqs (9), (11) and (12) into eq. (13) yields

$$B_d = \alpha \exp\left[\frac{E(\varepsilon_B - \varepsilon_A)}{\sigma_r + \sigma_3 - 2\mu\sigma_3 - E\varepsilon_A}\right] + \beta\left(1 - \frac{\sigma_r}{\sigma_a}\right) + \gamma\left[1 - \exp\left(\frac{M}{E}\right)\right]. \quad (14)$$

Validation of brittleness index parameters

In order to verify the validity of brittleness index B_d, the experimental results of Shuai *et al.*[40] were utilized. These experimental tests were carried out on MTS815 loading machine using axial displacement control, with a loading rate of 0.18 mm/min, and the confining pressure was set to 0, 10, 20 and 30 MPa. From the experimental results, relevant parameters were obtained, and then B_1, B_2 and B_3 were calculated based on eqs (9), (11) and (12). As shown in Table 2, if α, β and γ are given different values, we can get the corresponding B_d. By considering all the parameters from eq. (14), we can obtain the value of B_d as shown in Figure 9.

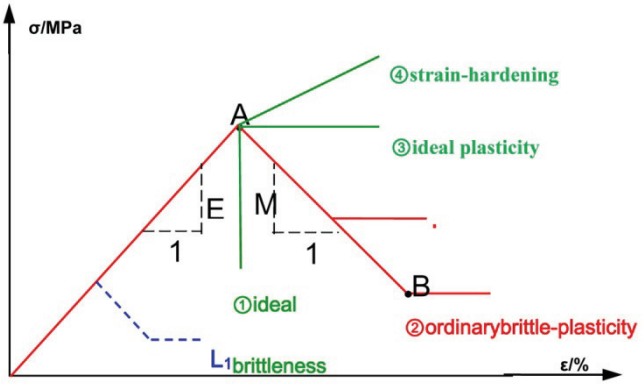

Figure 8. Classification of brittleness (hypothetical curve).

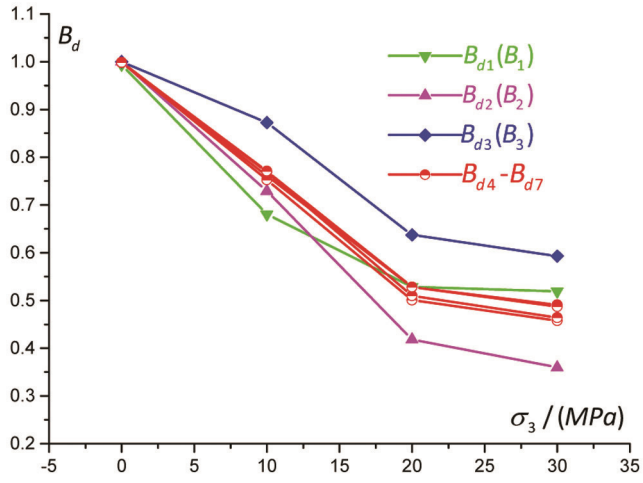

Figure 9. Average of the brittleness indices versus confining pressure curves.

Table 2. Brittleness index indices

Values of (α, β, γ)	Corresponding B_d
(1, 0, 0)	B_{d1}
(0, 1, 0)	B_{d2}
(0, 0, 1)	B_{d3}
(1/3, 1/3, 1/3)	B_{d4}
(1/4, 1/2, 1/4)	B_{d5}
(1/6, 1/2, 1/3)	B_{d6}
(1/4, 3/8, 3/8)	B_{d7}

As shown in Figure 9, the shale brittleness index B_d decreases with the increase of confining pressure σ_3 and drops more quickly under low confining pressure than at high pressure. Under low σ_3, B_d is more sensitive to σ_3 and a small pressure change can cause a rapid decrease of the brittleness index. However, under high pressure, the index is not sensitive and the change range is small. B_{d1}, B_{d2} and B_{d3} are the same as B_1, B_2 and B_3 respectively. They are the special cases of B_d and can individually reflect the shale brittleness. But their forms are relatively simple which tend to cause large errors. The indices B_{d4} and B_{d7} are general cases of B_d, which express the shale brittleness more comprehensively. They reduce the impact of experimental as well as data collection errors during the calculation of brittleness index. As shown in Figure 9, the curves for B_{d4} to B_{d7} are similar in their variation laws. Therefore, under normal circumstances, the brittleness index B_{d4} with $\alpha = \beta = \gamma = 1/3$ can be used to express the brittleness characteristics of shale.

Brittleness index of shale for different fracturing-fluid immersion times

Figure 10 shows the brittleness index of shale under different immersion times t. The brittleness index decreases with the increase of immersion time. When $t \le 72$ h, B_{d4} decreases linearly and is sensitive to immersion time. When $t \ge 72$ h, Bd_4 declines slowly, its range of change is small, and finally tends to a constant value. The indices B_{d1}, B_{d2} and B_{d3} also show similar variation with t. They individually reflect their shale brittleness, since their form is relatively simple and cause significant errors. Thus, B_{d4} is relatively superior and can express the brittle characteristics ore comprehensively. The average value of brittleness index B_{d4} has a significant exponential function with immersion time t, which can be explained as

$$B_{d4} = 0.562\exp(-t/23.692) + 0.142,\ R^2 = 0.985. \qquad (15)$$

From eq. (15), it is clear that with an infinite increase of immersion time, the shale brittleness index will eventually stabilize at 0.142.

Hydration swelling caused by fracturing-fluid causes damage to microstructure of shale, resulting in different degrees of degradation of macro-mechanical parameters. When the immersion time is less than 72 h, the macro-mechanical properties of shale, such as peak strength, residual strength, elastic modulus, softening modulus, Poisson's ratio and brittleness index change rapidly, showing a linear upward or downward trend. When the immersion time is more than 72 h, all the macro-mechanical parameters are relatively stable, their variation range is small, and they ultimately tend to a constant value. This shows that hydration swelling of shale is time-intensive and tends to be stable after about 72 h, which provides relevant parameters for studying the weakening mechanism of shale after soaking in fracturing-fluid.

Discussion on mechanisms of weakening of brittleness and mechanical properties of shale soaked in fracturing-fluid

Under the effect of soaking, fracturing-fluid enters into the voids of the shale along bedding planes and micro-cracks, and then advances rapidly by capillary force and hydration swelling stress. Micro-cracks form, extend and increase gradually, resulting in significant deterioration of mechanical properties and brittleness of shale. It is demonstrated that three factors can weaken the brittleness and mechanical parameters and these are discussed below.

Changes in stress state at the crack tip caused by fracturing-fluid

It is assumed that the shale sample contains elliptical cracks with the major axis of $2a$ as shown in Figure 11. In the micro-fracture, the length of the liquid column of the fracturing-fluid is $2b$ and the length of the infiltration

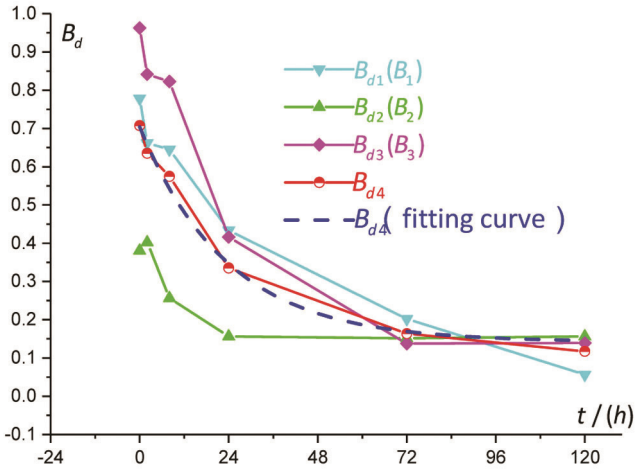

Figure 10. Average of the brittleness indices versus immersion time.

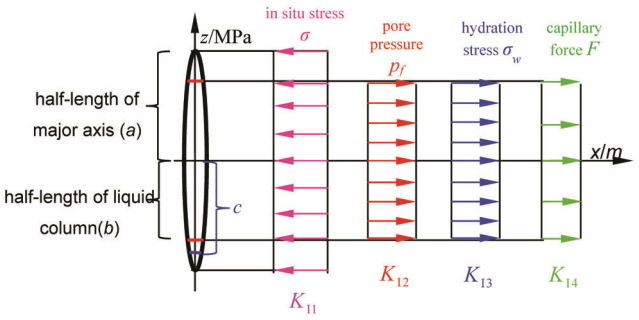

Figure 11. Stress and fracture toughness distributions at the crack-face.

zone is $2c$. Under the effect of fracturing-fluid infiltration, the stress intensity factor K_I at the crack tip is determined by *in situ* stress σ, pore pressure p_f, hydration stress σ_w and capillary force (F). Assuming that the individual stress intensity factors corresponding to the above four stresses are K_{I1}, K_{I2}, K_{I3} and K_{I4} respectively, the following equation can be obtained[6,41]

$$K_I = K_{I1} + K_{I2} + K_{I3} + K_{I4}. \quad (16)$$

If the *in situ* stress perpendicular to the fracture surface is σ and according to fracture mechanics, the stress intensity factor K_{I1} can be written as

$$K_{I1} = -\sigma\sqrt{\pi a}. \quad (17)$$

If the fluid pressure in the fracture is p_f, the stress intensity factor K_{I2} can be written as[41]

$$K_{I2} = 2p_f\sqrt{a/\pi}\arcsin(b/a). \quad (18)$$

Hydration stress is generated by the hydration swelling of clay minerals in shale. If the clay minerals are evenly distributed and the hydration stress acts evenly on the fracture surface, then using eq. (18), K_{I3} can be written as

$$K_{I3} = 2\sigma_w\sqrt{a/\pi}\arcsin(b/a), \quad (19)$$

where σ_w is the hydration stress acting on the crack surface.

Using Figure 12, the capillary force F is calculated as[42]

$$F = 2\gamma\cos(\theta-\beta)/\omega, \quad (20)$$

where γ is the interfacial tension for the fracturing-fluid, θ is the fluid contact angle, and β is the angle between the crack surface and long axis of the crack, 2ω is the aperture at the centre of the fracture and R is the equivalent radius of the fluid at the contact.

In Figure 12, the capillary force acting on the crack surface is $F\cos\theta$. Thus, K_{I4} under $F\cos\theta$ can be written as[6,42]

$$K_{I4} = \frac{4\gamma\cos(\theta)\cos(\theta-\beta)}{\omega}\sqrt{\frac{a}{\pi(a^2-c^2)}}, \quad (21)$$

where the length of the liquid column of fracturing-fluid is $2c$.

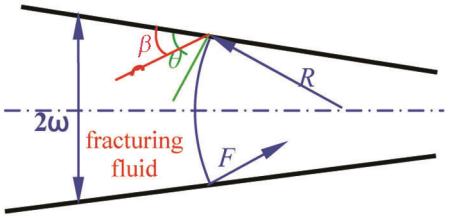

Figure 12. Capillary force at different locations in a fracture.

Substituting eqs (17)–(21) into eq. (16) yields

$$K_I = -\sigma\sqrt{\pi a} + 2(p_f+\sigma_w)\sqrt{\frac{a}{\pi}}\arcsin\left(\frac{b}{a}\right) + \frac{4\gamma\cos(\theta)\cos(\theta-\beta)}{\omega}\sqrt{\frac{a}{\pi\left(a^2-c^2\right)}}. \quad (22)$$

For immersion tests, since both the *in situ* stress σ and pore pressure p_f are almost zero, it can be concluded that both K_{I1} and K_{I2} are also almost zero. So in eq. (22), K_I is decided by K_{I3} and K_{I4}. According to the laboratory experiments, relevant parameters in eq. (22) can be considered as follows: $2a = 0.004$ m, $2c = 0.003$ m, $2b = 0.0002$ m, $2\omega = 0.000006$ m, $\gamma = 0.005$ N/m, $\theta = 30°$, $\beta = 0°$ and $\sigma_w = 1$ MPa. Using these values, the stress intensity factor $K_I = 0.98$ MPa m$^{1/2}$ is obtained. The fracture toughness K_{IC} parallel to and perpendicular to shale bedding planes are 0.57 MPa m$^{1/2}$ and 1.15 MPa m$^{1/2}$, respectively[43]. The value of K_I is comparatively larger than 0.57 and less than 1.15. Therefore, under the effect of fracturing-fluid soaking, micro-cracks extend only parallel to the bedding plane and rarely extend perpendicular to it.

Equation (22) shows significant positive linear correlations between K_I and σ, p_f, σ_w and γ, and an inversely proportional relationship between K_I and ω. For the immersion test, $\sigma = p_f = 0$, the relationships between K_I and $(b/a)(c/a)$ and θ are shown in Figure 13. When the immersion time is 0, $b = c = 0$ and $\theta = 90°$, K_I is small and insufficient to cause micro-cracks propagation. When immersion time is increased, $(b/a)(c/a)$ gradually increases and θ decreases, resulting in a gradual increase of K_I and increased stress concentration at the crack tip. When K_I at the crack tip reaches the fracture toughness K_{IC}, micro-cracks gradually develop and expand, resulting in a decrease in stiffness and strength of shale and a decline in post-peak stress decrease rate, eventually leading to the decline of brittleness and enhancement of plasticity.

Dissolution due to fracturing-fluid

Shale is rich in quartz, feldspar, clay minerals (such as illite and montmorillonite) and other silicate minerals. Under the action of alkaline fracturing-fluid, the following chemical reactions occur[44]

$$\text{Quartz: } SiO_2 + OH^- \rightarrow SiO_3^{2-} + H_2O,$$

$$\text{Orthoclase: } K[AlSi_3O_8] + OH^- \rightarrow K^+ + Al(OH)_3 + SiO_3^{2-},$$

$$\text{Illite: } K_{0.9}Al_{2.9}Si_{3.1}O_{10}(OH)_2 + nH_2O \rightarrow K_{0.9}Al_{2.9}Si_{3.1}O_{10}(OH)_2 \cdot nH_2O.$$

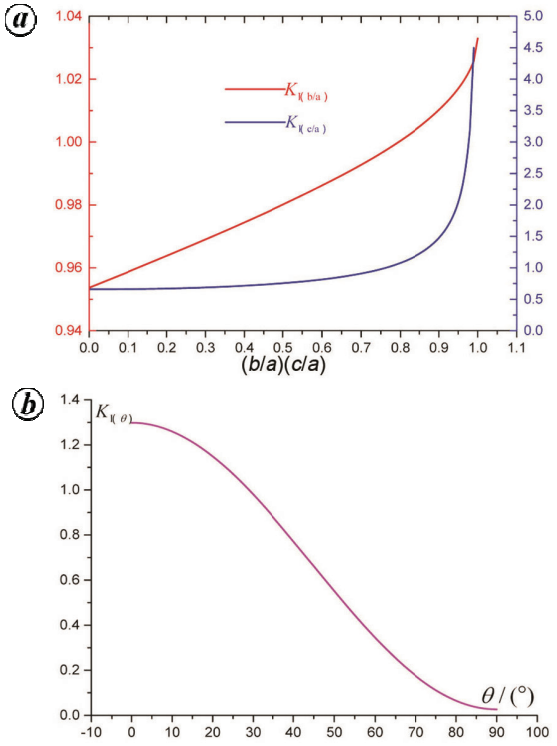

Figure 13. Effect of capillary on the stress intensity factor K_I; ***a***, Stress intensity factor versus $(b/a)(c/b)$; ***b***, Stress intensity factor versus contact angle.

The dissolution by fracturing-fluid causes a large number of dissolution pores in the shale, reduces the bonding strength between shale mineral grains significantly, changes the mineral composition of filler between bedding planes and decreases the frictional properties of fracture surface, internal friction angle and cohesion. The critical stress intensity factor is reduced by mineral erosion and structural damage of the crack tip[45]. All these make it easier for micro-cracks to expand. With increase of dissolved pores and micro-cracks, the brittleness of shale gradually decreases.

Lubrication due to fracturing-fluid

When the fracturing-fluid containing a quality fraction of 0.1% drag reducer enters the micro-cracks of shale, a liquid film forms on the surface of shale particles, which reduces the friction of crack surface and makes it more conducive to the expansion of cracks. The presence of liquid film helps the effective migration of proppant between cracks, which reduces the possibility of sand plugging. The liquid film significantly reduces the residual strength of shale and increases brittleness, which are both conducive to hydraulic fracturing.

In summary, due to the capillary imbibition, fracturing-fluid enters into the voids of shale along the bedding planes and micro-cracks. Due to the capillary force and hydration stress caused by the swelling of clay minerals when in contact with water, the stress intensity factor on the crack tip increases gradually. Under the effect of alkaline fracturing-fluid soaking, physical and chemical reactions take place between siliceous minerals and fracturing-fluid, which weaken the connection between mineral particles, resulting in a decrease in cohesion and internal friction angle. The critical stress intensity factor is reduced by mineral erosion and structural damage of the crack tip. The mechanical–physical–chemical multi-field coupling causes micro-cracks within shale to gradually develop and expand, resulting in a decrease in the strength and stiffness of the shale. Eventually, the brittleness of the shale is also strongly reduced.

Conclusion

The mechanical parameters of shale deteriorate significantly under the effect of fracturing-fluid soaking. The magnitudes of the degradation of peak strength, elastic modulus, softening modulus and residual strength are as high as 46.414%, 26.968%, 96.815% and 27.120% respectively. Hydration swelling of shale is time-intensive and tends to be stable after about 72 h. When the immersion time is less than 72 h, the macro-mechanical parameters of shale change rapidly, showing a linear upward or downward trend. However on the contrary, all the macro-mechanical parameters are relatively stable and ultimately tend to a constant value.

An evaluation of comprehensive brittleness index B_d is established based on the brittleness-drop coefficient, stress decrease coefficient and softening modulus. B_d has a significant exponential relation with immersion time t, and when $t \leq 72$ h, it decreases almost linearly with time. When $t \geq 72$ h, the decrease rate of B_d gradually slows down and it finally stabilizes at about 0.142.

Hydration swelling caused by clay minerals produces swelling stress and changes the internal stress state of shale, resulting in an increase of stress intensity factor at the crack tip. The dissolution by alkaline fracturing-fluid and a series of physical and chemical reactions between silica minerals and fracturing-fluid reduce the degree of cementation between bedding planes and the connection strength between shale mineral grains, diminish internal friction angle and cohesion, and decrease the critical stress intensity factor.

1. Administration, USEI, Technically recoverable shale oil and shale gas resources: an assessment of 137 shale formations in 41 countries outside the United States, 2013.
2. Hou, Z. K., Yang, C. H., Guo, Y. T., Zhang, B. P., Wei, Y. L., Shuai, H. and Lei, W., Experimental study on anisotropic properties of longmaxi formation shale under uniaxial compression. *Rock Soil Mech.*, 2015, **36**, 2541–2550.
3. Jarvie, D., Evaluation of hydrocarbon generation and storage in Barnett shale, Fort worth basin, Humble Geochmeical Services Division, Texas, 2004.
4. Guo, Y., Yang, C., Jia, C., Jingbin, X. U., Lei, W. and Dan, L. I., Research on hydraulic fracturing physical simulation of shale and fracture characterization methods. *Chin. J. Rock Mech. Eng.*, 2014, **33**, 52–59.

5. Hou, Z. K., Yang, C. H., Lei, W., Liu, P. J., Guo, Y. T., Wei, Y. L. and Zhi, L. I., Hydraulic fracture propagation of shale horizontal well by large-scale true triaxial physical simulation test. *Rock Soil Mech.*, 2016, **37**, 0407–0414.
6. Liang, L., Xiong, J. and Liu, X., Experimental study on crack propagation in shale formations considering hydration and wettability. *J. Nat. Gas Sci. Eng.*, 2015, **23**, 492–499.
7. Tianshou, M. A. and Chen, P., Study of meso-damage characteristics of shale hydration based on ct scanning technology. *Petrol. Exp. Dev.*, 2014, **41**, 249–256.
8. Wen, H., Chen, M., Jin, Y., Wang, K., Xia, Y., Dong, J. and Niu, C., A chemo-mechanical coupling model of deviated borehole stability in hard brittle shale. *Petrol. Exp. Dev.*, 2014, **41**, 817–823.
9. Ma, T., Yang, C., Chen, P., Wang, X. and Guo, Y., On the damage constitutive model for hydrated shale using ct scanning technology. *J. Nat. Gas Sci. Eng.*, 2016, **28**, 204–214.
10. Han, Q., Chen, P. and Ma, T., Influencing factor analysis of shale microindentation measurement. *J. Nat. Gas Sci. Eng.*, 2015, **27**, 641–650.
11. Yan, Z., Xiang, X., Yan, J. and Wu, B., A novel drilling fluid with less free water. *Petrol. Exp. Dev.*, 2011, **38**, 490–494.
12. Zhong, H., Qiu, Z., Zhang, D., Tang, Z., Huang, W. and Wang, W., Inhibiting shale hydration and dispersion with amine-terminated polyamidoamine dendrimers. *J. Nat. Gas Sci. Eng*., 2016, **28**, 52–60.
13. Younessi, A. and Rasouli, V., A fracture sliding potential index for wellbore stability analysis. *Int. J. Rock Mech. Mining Sci.*, 2010, **47**, 927–939.
14. Lomba, R. F. T., Chenevert, M. E. and Sharma, M. M., The role of osmotic effects in fluid flow through shales. *J. Petrol. Sci. Eng.*, 2000, **25**, 25–35.
15. Oort, E. V., On the physical and chemical stability of shales. *J. Petrol. Sci. Eng.*, 2003, **38**, 213–235.
16. Kang, Z. Q., Zhao, Y. S., Meng, Q. R., Yang, D. and Xi, B. P., Micro-ct experimental research of oil shale thermal cracking laws. *Chin. J. Geophys.*, 2009, **52**, 842–848.
17. Guancheng, J., Yourong, Q., Yuxiu, A., Xianbin, H. and Yanjun, R., Polyethyleneimine as shale inhibitor in drilling fluid. *Appl. Clay Sci.*, 2016, **127–128**, 70–77.
18. Shadizadeh, S. R., Moslemizadeh, A. and Dezaki, A. S., A novel nonionic surfactant for inhibiting shale hydration. *Appl. Clay Sci.*, 2015, **118**, 74–86.
19. Wang, P. and Qu, Z., NMR technology based hydration damage evolution of hard brittle shale. *Rock Soil Mech.*, 2015, **36**, 687–693.
20. Josh, M., Esteban, L., Piane, C. D., Sarout, J., Dewhurst, D. N. and Clennell, M. B., Laboratory characterization of shale properties. *J. Petrol. Sci. Eng.*, 2012, **88–89**(2), 107–124.
21. Wu, X. Y., Baud, P. and Wong, T. F., Micromechanics of compressive failure and spatial evolution of anisotropic damage in darley dale sandstone. *Int. J. Rock Mech. Min. Sci.*, 2000, **37**, 143–160.
22. Wang, F. and Pan, Z., Numerical simulation of chemical potential dominated fracturing fluid flowback in hydraulically fractured shale gas reservoirs. *Petrol. Exp. Dev.*, 2016, **43**, 1060–1066.
23. Zou, C. *et al.*, Shale gas in china: Characteristics, challenges and prospects (ii). *Petrol. Exp. Dev.*, 2015, **43**, 182–196.
24. Lu, Y. H., Chen, M., Jin, Y. and Zhang, G. Q., A mechanical model of borehole stability for weak plane formation under porous flow. *Liq. Fuels Technol.*, 2012, **30**, 1629–1638.
25. Wang, Y., Xiao, L. I., Yanfang, W. U., Yuxing, B., Shouding, L. I., Jianming, H. E. and Zhang, B., Research on relationship between crack initiation stress level and brittleness indices for brittle rocks. *Chin. J. Rock Mech. Eng.*, 2014, **33**(2), 264–275.
26. Hou, Z. K., Yang, C. H., Wei, X., Wang, L., Wei, Y. L., Xu, F. and Wang, H., Experimental study on the brittle characteristics of longmaxi formation shale. *J. China Coal Soc.*, 2016, **41**, 1188–1196.
27. Hucka, V. and Das, B., Brittleness determination of rocks by different methods. *Int. J. Rock Mech. Min. Sci. Geomech. Abstracts*, 1974, **11**, 389–392.
28. Hou, Z. K., Yang, C. H., Wang, L. and Feng, X. U., Evaluation method of shale brittleness based on indoor experiments. *J. Northeastern Univ.*, 2016, **37**, 1496–1501.
29. Kahraman, S. and Altindag, R., A brittleness index to estimate fracture toughness. *Int. J. Rock Mech. Min. Sci.*, 2004, **41**, 343–348.
30. Qinghui, L. I., Chen, M., Yan, J., Wang, F. P., Bing, H. and Zhang, B., Indoor evaluation method for shale brittleness and improvement. *Chin. J. Rock Mech. Eng.*, 2012, **31**, 1680–1685.
31. Xu, F. *et al.*, Effect of bedding planes on wave velocity and ae characteristics of the longmaxi shale in china. *Arab. J. Geosci.*, 2017, **10**, 141.
32. Hui, Z., Meng, F., Zhang, C., Rongchao, X. U. and Jingjing, L. U., Quantitative evaluation of rock brittleness based on stress-strain curve. *Chin. J. Rock Mech. Eng.*, 2014, **33**, 1114–1122.
33. Kang, Y., She, J., Lin, C. and You, L., Brittleness weakening mechanisms of shale soaked by drilling and completion fluid. *Chin. J. Theoret. Appl. Mech.*, 2016, **48**, 730–738.
34. GT/T23561-2009, The Professional Standards Compilation Group of Peoples Republic of China, Methods for determining the physical and mechanical properties of coal and rock. Standards Press of China, Beijing, 2009.
35. Wang, H., Guo, Y. T., Wang, L., Hou, Z. K. and Xu, F., An experimental study on mechanical anisotropy of shale reservoirs at different depths. *Rock Soil Mech.*, 2017, **38**, 2496–2506.
36. Arora, S. and Mishra, B., Investigation of the failure mode of shale rocks in biaxial and triaxial compression tests. *Int. J. Rock Mech. Min. Sci.*, 2015, **79**, 109–123.
37. Shi, G., Research on post-failure mechanical properties of brittle-plastic rocks by OOFEM coupled with IEM. Doc. Diss., University of Chinese Academy of Sciences, 2005.
38. Zuo, J. *et al.*, Study of energy-drop coefficient of brittle rock failure. *Rock Soil Mech.*, 2014, **35**(2), 321–327.
39. Obert, L. and Duvall, W. I., *Rock Mechanics and the Design of Structures in Rock*, John Wiley, Chichester, 1996, p. 649.
40. Shuai, H., Yang, C., Zhi, L. I., Lei, W. and Hou, Z., Shale brittleness estimation based on energy dissipation. *J. Central South Univ.*, 2016.
41. Liu, X., Zeng, W., Liang, L. and Xiong, J., Experimental study on hydration damage mechanism of shale from the longmaxi formation in southern Sichuan basin, China. *Petroleum*, 2016, **2**, 54–60.
42. Yang, S. L. and Wei, J. Z., *Reservoir Physics*, Petroleum Industry Press, Beijing, 2004.
43. Shuai, H., Yang, C., Guo, Y., Wang, C. and Lei, W., Influence of bedding planes on hydraulic fracture propagation in shale formations. *Chin. J. Rock Mech. Eng.*, 2015, **34**, 228–237.
44. Kang, Y., Chen, Q., You, L., Lin, C. and Cheng, Q., Laboratory studies of shale fracturing behaviors with rock-drilling fluid interactions, 2016, **40**, 81–89.
45. You, L., Kang, Y., Chen, Z., Chen, Q. and Yang, B., Wellbore instability in shale gas wells drilled by oil-based fluids. *Int. J. Rock Mech. Min. Sci.*, 2014, **72**, 294–299.

ACKNOWLEDGEMENTS. This work was supported by Study on Formation Mechanism and Extended Model of Complex Fracture Network in Shale Gas Reservoir (the National Natural Science Foundation of China, No. 51574218), Study on Stress and Strain Characteristics of Roof and Floor of Shale Reservoir (National Science and Technology Major Project of China, No. 2017ZX05036-003), Study on Rock Mechanics Property of Shale and Complex Fracture Law of Hydraulic Fracturing (National Science and Technology Major Project of China, No. 2016ZX05060-004), Experimental Study on Working Mechanism of Rockburst Prevention Anchoring System (National Natural Science Foundation of China, Grant No. 51709113), Research on Support Theory and Technique of Dynamic Disaster Prevention in Deep Rock mass (the Science and Technology Project of Henan Province, Grant No. 172102310475) and Evolution Mechanism of the Landslide with the Potential Locked Section and its Dynamic-tracking early Warning Method in the Western Henan Province (Grant No. U1704243).

Received 30 April 2017; revised accepted 9 January 2018

doi: 10.18520/cs/v115/i6/1163-1173